Exclusive η production in proton-proton reactions

F. Balestra,[1] Y. Bedfer,[2,*] R. Bertini,[1,2] L. C. Bland,[3] A. Brenschede,[4,†] F. Brochard,[2,‡] M. P. Bussa,[1] Seonho Choi,[3,§] M. L. Colantoni,[1] R. Dressler,[6,‖] M. Dzemidzic,[3,¶] J.-Cl. Faivre,[2,†] A. Ferrero,[1] L. Ferrero,[1] J. Foryciarz,[9,5,**] I. Fröhlich,[4] V. Frolov,[7,††] R. Garfagnini,[1] A. Grasso,[1] S. Heinz,[1,2] W. W. Jacobs,[3] W. Kühn,[4] A. Maggiora,[1] M. Maggiora,[1] A. Manara,[1,2] D. Panzieri,[8] H.-W. Pfaff,[4,‡‡] G. Piragino,[1] A. Popov,[7] J. Ritman,[4] P. Salabura,[5] V. Tchalyshev,[7] F. Tosello,[1] S. E. Vigdor,[3] and G. Zosi[1]

(DISTO Collaboration)

[1]*Dipartimento di Fisica "A. Avogadro" and INFN, Torino, Italy*

[2]*Laboratoire National Saturne, CEA Saclay, France*

[3]*Indiana University Cyclotron Facility, Bloomington, Indiana 47408, USA*

[4]*II. Physikalisches Institut, University of Gießen, Gießen, Germany*

[5]*M. Smoluchowski Institute of Physics, Jagellonian University, Kraków, Poland*

[6]*Forschungszentrum Rossendorf, Rossendorf, Germany*

[7]*JINR, Dubna, Russia*

[8]*Universita' del Piemonte Orientale and INFN, Torino, Italy*

[9]*H. Niewodniczanski Institute of Nuclear Physics, Kraków, Poland*

(Received 30 April 2003; published 28 June 2004)

Differential cross sections for the exclusive reaction $\vec{p}p \to pp\eta$ observed via the $\eta \to \pi^+\pi^-\pi^0$ decay channel have been measured at $T_{\mathrm{beam}} = 2.15$ GeV, 2.50 GeV, and 2.85 GeV (excess energies 324 MeV, 412 MeV, and 554 MeV). The influence of the $N(1535)S_{11}$ resonance is clearly seen in the invariant mass and momentum dependent differential cross sections. The extracted resonance parameters are compatible with existing data. No significant evidence for further resonance contributions has been found. In addition, angular distributions of the $pp\eta$ final state have been measured. The polar angle distribution of the η shows an anisotropy with respect to the beam axis for the lowest beam energy, which vanishes for the higher energies. The sign of this anisotropy is negative and expected to be sensitive to the dominant production mechanism. In contrast, the proton polar angle in the *pp* rest frame tends to be more strongly aligned along the beam axis with increasing beam energy. The analyzing power A_y is compatible with zero for all beam energies.

DOI: 10.1103/PhysRevC.69.064003 PACS number(s): 13.75.Cs, 25.40.Ve, 14.40.Aq

I. INTRODUCTION

In recent years the production of η mesons in proton-proton reactions has raised significant interest both experimentally and theoretically, since modern techniques allow to determine total and differential cross sections more precisely. After early bubble chamber experiments [1] that measured total cross sections, in the last decade a new series of experiments have provided high statistics data in the near threshold region with beam energies of less than 2 GeV at SATURNE II [2–4], CELSIUS [5,6], and COSY [7–10]. These data have been interpreted in the framework of one-boson exchange models [11–17], which differ in predictions for the dominant contribution of the η, π, ρ, and ω exchange mesons. The general conclusion was that the knowledge of the total cross section is not sufficient for a clear discrimination of the contribution of the individual mesons and therefore differential cross sections and/or polarization observables such as the analyzing power are needed.

At CELSIUS [6], angular distributions of the η emission in the center-of-mass (c.m.) system as well as for the protons in the *pp* rest frame have been measured in proton-proton collisions at near threshold energies (excess energies $Q = \sqrt{s - s_0} = 16$ and 37 MeV). It has been shown that the η differential cross section as a function of the η c.m. polar angle $\theta_\eta^{\mathrm{c.m.}}$ is not isotropic and shows a maximum of emitted η mesons perpendicular to the beam direction. The angular distribution measurement at COSY [10] at similar excess energies shows, however, no deviation from isotropy, which is in contradiction to the measurement at CELSIUS. The data measured with the SPES-3 spectrometer at SATURNE II [4] at a larger excess energy $Q = 100$ MeV show a strong forward peaking of the produced η mesons. In addition, there are data on the analyzing power A_y available measured with SPES-3 and at COSY [9].

*Present address: DAPNIA/SPhN, CEA Saclay, France.

†Present address: DIAMOS AG, Sulzbach, Germany.

‡Present address: LPHNHE, Ecole Polytechnique 91128 Palaiseau, France.

§Present address: Temple Univ., Philadelphia, Pennsylvania, USA.

‖Present address: Paul Scherrer Institut, Villigen, CH-5232, Switzerland.

¶Present address: IU School of Medicine, Indianapolis, Indiana, USA.

**Present address: Motorola Polska Software Center, Kraków, Poland.

††Present address: Dipartimento di Fisica "A. Avogadro" and INFN, Torino, Italy.

‡‡Present address: D-fine GmbH, 65760 Eschborn, Frankfurt, Germany.

The shape of the angular distributions measured at CELSIUS has been interpreted by Fäldt and Wilkin [16] as due to a dominant excitation of the $N(1535)S_{11}$ by the exchange of ρ vector mesons with destructive ρ/π interference. The angular distributions should be forward peaked if π exchange would be dominant. In a recent calculation of Nakayama *et al.* [17], however, it has been shown that this shape could as well be explained by a excitation of the resonance by pseudoscalar mesons with mesonic current interference. Since both scenarios, the dominant pseudoscalar and vector meson exchange, lead to similar predictions for the angular distributions, additional data such as the analyzing power A_y as a function of $\cos(\theta_\eta^{\text{c.m.}})$ are needed to disentangle these two scenarios. In this context, the COSY data on the analyzing power at $Q=40$ MeV [9] seem to favor vector meson exchange.

For excess energies larger than $Q=100$ MeV, no differential cross sections have been measured so far. Such measurements are needed to investigate the contributions of the individual exchange mesons at higher energies where final state interactions are small.

In addition, detailed knowledge of the η production mechanism is important for the interpretation of the $N(1535)S_{11}$ resonance which has a large branching ratio into $p\eta$ of 30–55% [18] and a mass pole slightly above the $p\eta$ threshold. Despite theoretical efforts [19] to understand this large coupling to the η channel of the $N(1535)S_{11}$, the underlying structure of this resonance is still not clear.

In this paper, differential cross sections for the exclusive reaction $\vec{p}p\to pp\eta$ are presented, which have been measured with the DISTO spectrometer [20] at $Q=324$ MeV, 412 MeV, and 554 MeV. First, an overview of the apparatus and the data analysis techniques are given. In the second part, the $p\eta$ invariant mass, momentum, and angular differential cross sections as well as the analyzing power are presented.

II. EXPERIMENT

A. Apparatus

The DISTO magnetic spectrometer was located at the SATURNE II accelerator. Polarized proton beams with kinetic energies of 2.15 GeV, 2.50 GeV, and 2.85 GeV were directed to a liquid hydrogen target. The detector consisted of a large dipole magnet which covered the target as well as two sets of scintillating fiber arrays. Outside the magnetic field, two sets of multiwire proportional chambers (MWPC) were mounted, along with segmented plastic scintillator hodoscopes and water Čerenkov detectors. The large solid angle of the detector allowed final states with four charged particles to be measured. It should be remarked that under the same conditions of four charged particles in the final state various reactions have been measured simultaneously, like ppK^+K^-, $pp\pi^+\pi^-(\pi^0)$, and pKY, $Y=\Sigma,\Lambda$ [21–23]. The hodoscope and the fiber arrays were used for the trigger condition whereas the MWPC and the water Čerenkov detectors were employed for momentum determination and particle identification, which allowed a separation of protons and pions over the relevant large momentum range.

B. Data analysis

Exclusive η production has been observed via the kinematically overdetermined reaction $pp\to pp\eta\to pp\pi^+\pi^-\pi^0$ (branching ratio $22.6\pm0.4\%$ [18]). The three-momentum of each charged particle has been calculated from its deflection in the magnetic field. The tracks were reconstructed using the hit pattern information of the MWPC. In order to get the four-momentum vector, the protons and charged pions in the final state have been identified and assigned to the individual tracks.

The particle identification was performed by applying a mass hypothesis to each particle simultaneously. This method selects the hypothesis with the minimum joint χ^2 value which is calculated for each possible combination of the measured tracks to the expected charged particles in the final state ($pp\pi^+\pi^-$). We calculated the χ^2 by comparing the measured Čerenkov light output to the expected value based on the mass hypothesis and the three-momentum. The lowest χ^2 has been used to assign the particle masses to the tracks. The condition on $\chi^2_{\text{best}}/NDF<3$, where NDF is the number tracks with Čerenkov light output, has been set. This selection suppresses background from events with other particles in the final state and incorrectly reconstructed events of the type $pp\pi^+\pi^-$. It has been determined by means of Monte Carlo simulations that less than 7% of the remaining events have been incorrectly reconstructed.

After the identification of all four charged particles in the final state, energy and momentum conservation can be used to reconstruct the invariant mass M_X^{inv} and missing mass M_X^{miss} of individual particle combinations X in the final state. In order to enhance the $pp\pi^+\pi^-\pi^0$ final state compared to the dominant reaction channel $pp\to pp\pi^+\pi^-$, a missing π^0 has been selected by requiring $0.002\ \text{GeV}^2/c^4<(M^{\text{miss}}_{pp\pi^+\pi^-})^2<0.037\ \text{GeV}^2/c^4$ and $(M^{\text{inv}}_{\pi^+\pi^-})^2<(M^{\text{miss}}_{pp})^2$. These selection criteria improved the signal-to-background ratio by over a factor of 4 at the expense of a 40% reduction of the signal. It has been confirmed that the results presented below are not significantly affected by 30% changes to the $(M^{\text{miss}}_{pp\pi^+\pi^-})^2$ selection range. A further suppression of background and gain in resolution has been achieved by a kinematic refit, where the momenta of all four tracks have been redetermined with the additional constraint that $M^{\text{miss}}_{pp\pi^+\pi^-}=M_{\pi^0}$ [22].

The acceptance of the detector has been determined by means of the Monte Carlo simulations, which were processed through the same analysis chain as the measured data. The simulations indicate a very low acceptance of the apparatus for events in which the η were produced in the backward hemisphere in the c.m. reference frame. However, since the initial system consists of two identical particles, a reflection symmetry about $\theta^{\text{c.m.}}=90°$ exists, thus the backward data are redundant for the cross section determination. In the forward hemisphere the detector acceptance was found to be nonzero over the full kinematically allowed region after taking all symmetries into account, thus eliminating the need for

model dependent extrapolations of the cross section into unmeasured regions of phase space. The data presented below have been corrected on an event-by-event basis via a weighting factor as a function of all relevant variables.

The three body $pp\eta$ final state can be fully described by five independent variables. We have chosen the invariant masses $M^{\mathrm{inv}}_{p_1\eta}$, $M^{\mathrm{inv}}_{p_2\eta}$ and three Euler angles to fully parametrize the three body final state. Two of these three angles are the azimuthal and polar angles ($\phi^{\mathrm{c.m.}}_{\eta}$ and $\theta^{\mathrm{c.m.}}_{\eta}$) of the η c.m. momentum vector. The third angle ($\psi^{\mathrm{c.m.}}_{pp}$) describes the additional rotation of the decay plane about the axis defined by the η c.m. momentum vector. For the differential cross sections, the $\phi^{\mathrm{c.m.}}_{\eta}$ distribution must be isotropic for symmetry reasons because we integrate over both beam polarization directions and the relative luminosities were equal. Therefore the kinematically allowed phase space has been divided into four-dimensional kinematic bins, corresponding to the remaining independent variables $M^{\mathrm{inv}}_{p_1\eta}$, $M^{\mathrm{inv}}_{p_2\eta}$, $\theta^{\mathrm{c.m.}}_{\eta}$, and $\psi^{\mathrm{c.m.}}_{pp}$. However, for the determination of the spin-dependent observables we included $\phi^{\mathrm{c.m.}}_{\eta}$ as an additional dimension in our matrix. The efficiency correction factor was determined for each bin separately by dividing the number of generated $pp\eta$ events by the number of reconstructed events in the corresponding acceptance bin. It has been shown that this method is independent of the primary distribution used by the event generator. For a detailed discussion see Ref. [23].

After all selection conditions, the data still contain background from nonresonant $\pi^+\pi^-\pi^0$ production. In order to extract the η yield, the pp missing mass spectrum was analyzed via a χ^2 minimization routine with a function describing the resonant η shape and nonresonant contributions. The background has been parametrized by a polynomial. The line shape of the η signal was derived from Monte Carlo simulation for each individual bin of the corresponding observable. Figure 1 shows the M^{miss}_{pp} differential cross section for four ranges of the polar angle of the η meson in the c.m. system at each beam energy after correction for detector acceptance.

Due to the large systematic uncertainty of the beam current normalization, we do not provide values for the total cross section for the $pp\rightarrow pp\eta$ reaction. However, a large amount of data on the total cross section for this reaction are known from many other experiments, allowing us to obtain the absolute normalization of our data, as shown in Ref. [23]. The values of the total cross sections used to normalize our data were $85\pm20\mu$b, $115\pm30\mu$b, and $135\pm35\mu$b for the $T_{\mathrm{beam}}=2.15$ GeV, 2.50 GeV, and 2.85 GeV beam energies, respectively. Since the absolute normalization enters only as a global scale, the related error bars have not been included in the errors of the individual bins in the data presented here.

Each bin of the differential cross sections has an individual error due to systematic effects, which are dominated by the acceptance correction and background subtraction. To evaluate the bin-by-bin errors, both the statistical error from the minimization routine and the bin-by-bin systematical error have been taken into account. The systematic error has been obtained by comparing different background parametrizations with similar χ^2 values and is included in all differential cross sections presented in this work.

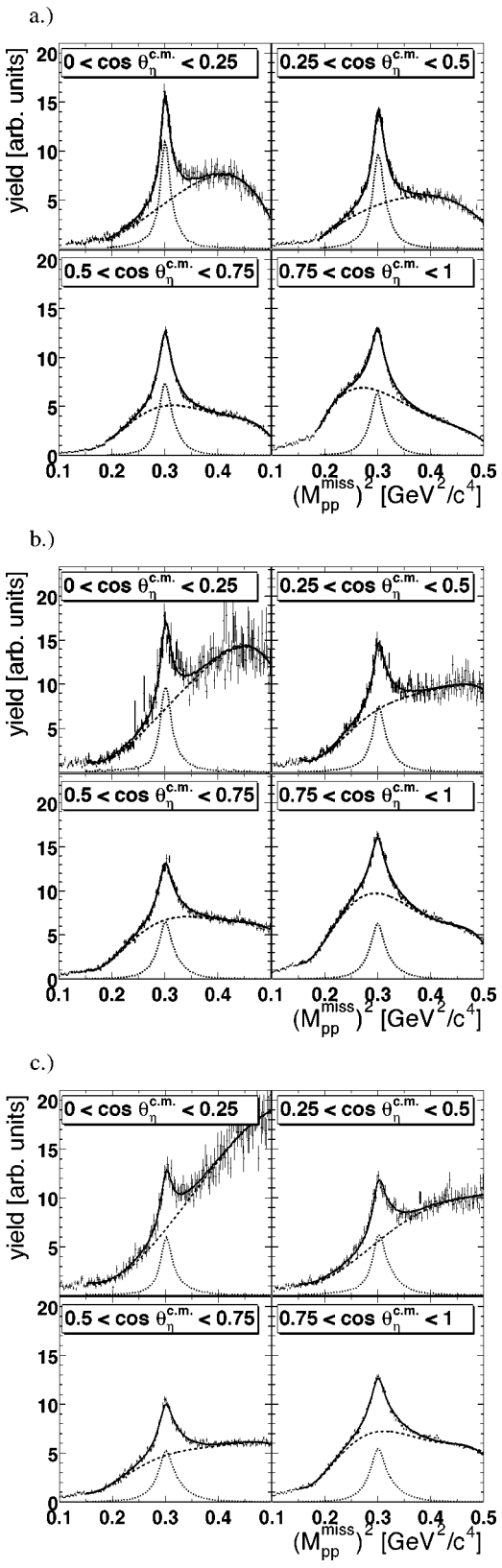

FIG. 1. Differential cross sections of the proton-proton missing mass squared for four different cos $\theta^{\mathrm{c.m.}}_{\eta}$ ranges before absolute normalization (a) 2.15 GeV, (b) 2.50 GeV, and (c) 2.85 GeV data. Dotted line: η line shape from Monte Carlo simulation. Dashed line: polynomial background. Solid line: signal plus background.

C. Experimental results

1. Dalitz plots and invariant mass spectra

The presentation of the data in the Dalitz plot is a powerful method to investigate structures in the $pp\eta$ system, such as the excitation of N^* resonances and final state interactions. One possible choice of the invariant mass combinations is $M^{\mathrm{inv}}_{p_1\eta}$ and $M^{\mathrm{inv}}_{p_2\eta}$. Figure 2 shows Dalitz plots for all three beam energies, where the yield in each phase space bin has been evaluated as described above. The solid curve represents the kinematic limits of the reaction. In order to correct for effects due to the kinematic limit, the bins at the edge have been divided by the fraction of the kinematic allowed region within this bin. The data points that appear to be outside the kinematic limit arise from the finite bin size.

All Dalitz plots show a clear enhancement at the $p\eta$ threshold, which can be assigned to the $N(1535)S_{11}$ resonance. This signal is in agreement with S-wave behavior of the $N(1535)S_{11}$ and consistent with a width of 100−200 MeV [18]. Since both outgoing protons p_1 and p_2 are randomly selected by the analysis procedure, the Dalitz plots have a reflection symmetry with respect to the diagonal.

Due to the limited detector acceptance, protons from the decay of the $N(1535)S_{11}$ are predominantly observed in the forward c.m. hemisphere. Thus, the proton-η combination most likely originating from the $N(1535)S_{11}$ can be determined by sorting the outgoing protons according to the absolute value of the four-momentum transfer $|t|$ from the incoming beam proton to each of the outgoing protons. The final state protons are now labeled $p_<$ and $p_>$ such that $|t(p_<)| < |t(p_>)|$, and the invariant masses of the $p\eta$ systems are now denoted as $M^{\mathrm{inv}}_{p_<\eta}$ and $M^{\mathrm{inv}}_{p_>\eta}$. Figure 3 shows the invariant mass distribution $M^{\mathrm{inv}}_{p_<\eta}$, divided by the volume of available phase space, which is proportional to the square of the decay matrix element $|M|^2$ of the $p_<\eta$ system. All data sets at our three beam energies are in agreement within the errors. The data points have been normalized by setting the integral in the range $1.485 < M^{\mathrm{inv}}_{p_<\eta} < 1.81$ GeV/c^2 to the same value.

As pointed out in Ref. [24], the deviation from $|M|^2$ due to the near-threshold resonance $N(1535)S_{11}$ can be described by a Breit-Wigner distribution

$$\sigma(M) = \frac{A M_R^2 \Gamma_R^2}{(M_R^2 - M^2)^2 + M_R^2 \Gamma_R^2 x(M, M_R)}, \qquad (1)$$

where M_R and Γ_R are the resonance mass and width, and x is the correction

$$x = b_\eta \frac{q_\eta(M)}{q_\eta(M_R)} + b_\pi \frac{q_\pi(M)}{q_\pi(M_R)} + b_{\pi\pi}, \qquad (2)$$

for the energy dependent width. The parameters $q_{\eta,\pi}(M)$ are the c.m. momenta of the respective mesons. The branching ratios have been set to $b_\eta = 0.55$, $b_\pi = 0.45$, and $b_{\pi\pi} = 0$ as in Ref. [24]. It should be noted that a possible modification of the fit results due to the uncertainties of these branching ratios is much smaller than the statistical error from the fit to the data. The best fit result is presented as the solid line in Fig. 3 with the result $M_R = 1530 \pm 7$ MeV/c^2 and $\Gamma_R = 120 \pm 30$ MeV/c^2. However, the shape of the fit function using the parameters $M_R = 1540$ MeV/c^2 and $\Gamma_R = 150$ MeV/c^2, taken from photoproduction data which cov-

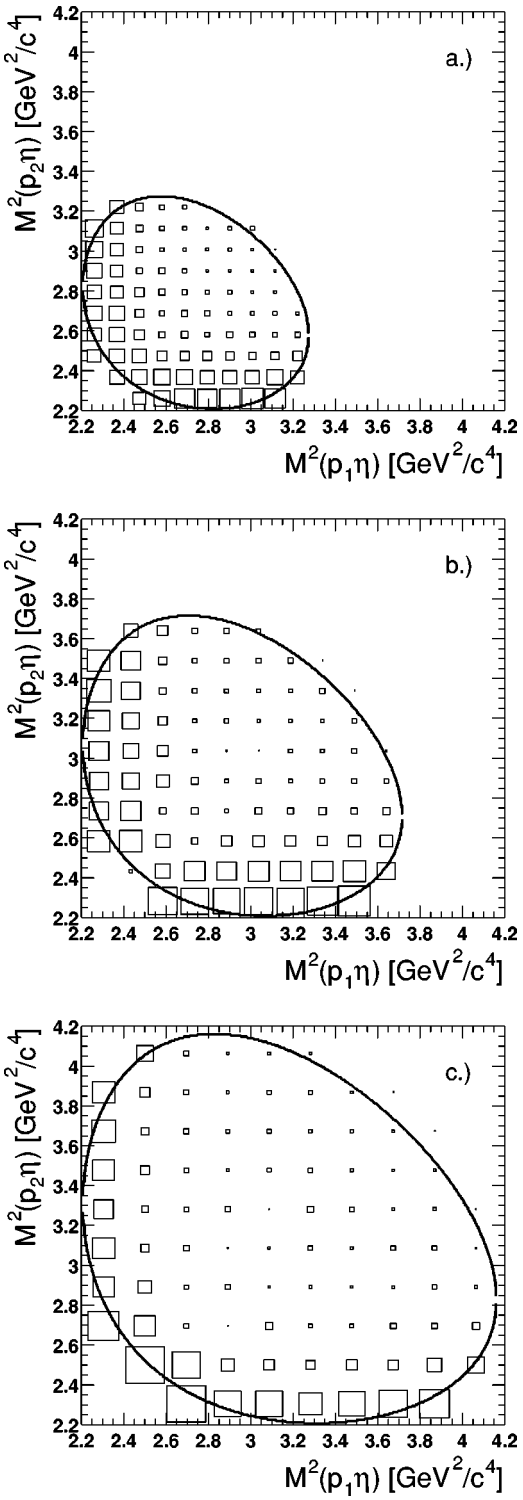

FIG. 2. Dalitz plots for all three kinetic beam energies (a) 2.15 GeV, (b) 2.50 GeV, (c) 2.85 GeV. The solid curves indicate the corresponding kinematical limits.

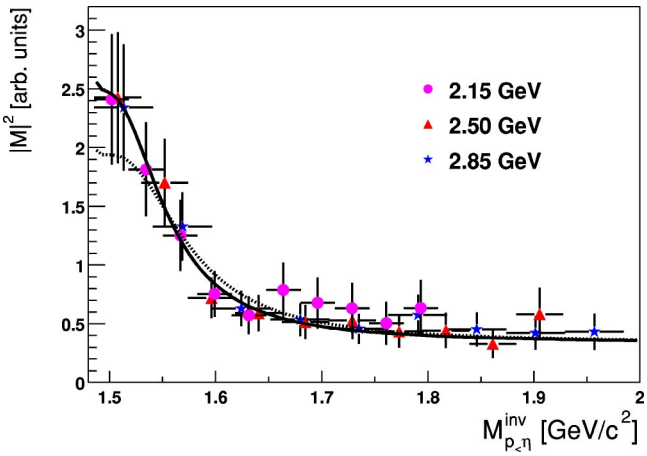

FIG. 3. (Color online) Differential cross section divided by the phase space as a function of the invariant mass $M^{\mathrm{inv}}_{p<\eta}$. The solid curve is a fit using formula (1) and the dotted line shows the same function but with the resonance parameters taken from Ref. [25].

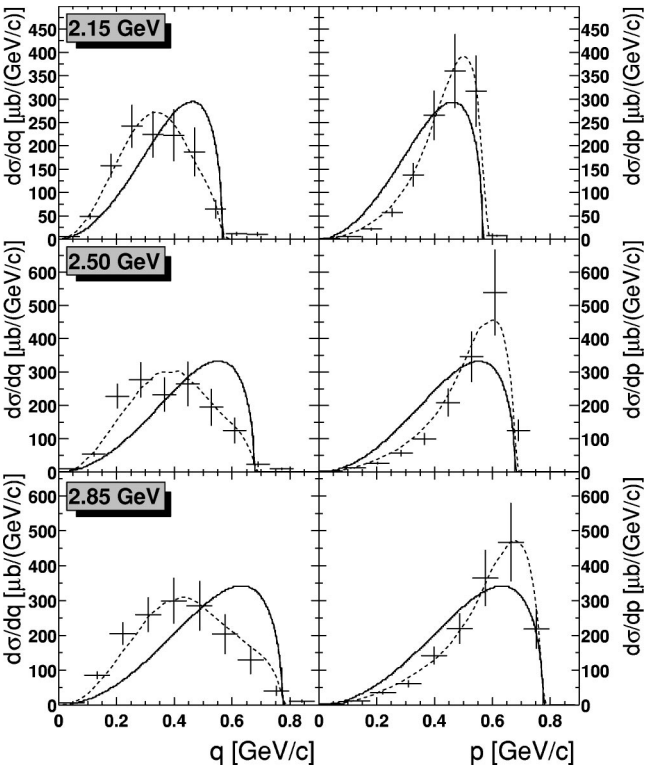

FIG. 4. Differential cross sections vs the c.m. momentum of the η meson (q, left column) and vs the proton momentum p in the pp rest frame (right column) compared to simulations based on equal s-wave phase space population (solid curve) and simulations including the $N(1535)S_{11}$ contribution with the parameters from our Breit-Wigner fit (dashed histogram). The error bars include both statistical and the relative systematical uncertainties, but do not include the global uncertainty of the absolute scale.

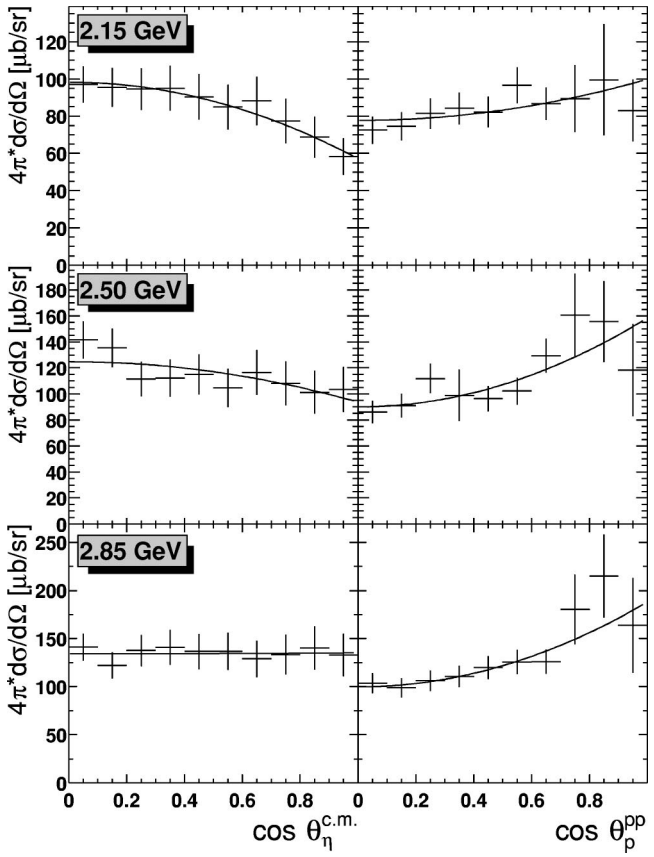

FIG. 5. Angular distributions of the η with respect to the beam direction (left column) and of the pp system in the pp rest frame (right column). The solid line as a fit with the first two even Legendre polynomials. The error bars include both statistical and the relative systematical uncertainties, but do not include the global uncertainty of the absolute scale.

ered the full resonance signal [25], is still within 2σ of our data.

2. Momentum differential cross sections

In addition to the invariant masses as used in the Dalitz plot, two independent momenta can be used to describe the internal motion of a three body final state. Here, we have selected the momentum of the η meson in the c.m. system $\vec{q}$ and the momentum of a proton in the pp rest frame $\vec{p}$. A projection of the yield onto p and q allows a sensitive test for the presence of higher partial waves [26] in the cross section not associated with the $N(1535)S_{11}$. Figure 4 shows these

TABLE I. Summary of the fit parameters to the angular distributions for the measured beam energies T_{beam} and excess energies Q.

T_{beam}(GeV)	Q(MeV)	$c_2(\eta)$	$c_2(pp)$
2.15	324	-0.32 ± 0.10	0.17 ± 0.12
2.50	412	-0.18 ± 0.11	0.40 ± 0.15
2.85	554	-0.01 ± 0.10	0.46 ± 0.15

TABLE II. Summary of the analyzing power and the fit result to formula 5 for the measured beam energies T_{beam} and excess energies Q.

T_{beam}(GeV)	Q(MeV)	A_y	A_y^{max}
2.15	324	0.13±0.10	0.28±0.17
2.50	412	0.03±0.12	0.00±0.11
2.85	554	0.10±0.12	0.10±0.16

momentum differential cross sections compared to Monte Carlo simulations. The solid line represents equal *s*-wave population of the available phase space and the dashed line accounts for our observed $M^{\mathrm{inv}}_{p<\eta}$ distribution parametrized by the Breit-Wigner fit in Fig. 3. The errors of the absolute normalization of 22%, 30%, and 33% for the T_{beam} = 2.15 GeV, 2.50 GeV, and 2.85 GeV beam energies, are not included in this figure.

It can be seen that the momentum differential cross sections exhibit a strong influence of the resonance signal and differ clearly from phase space, as already pointed out by Vetter *et al.* [12]. Beside the $N(1535)S_{11}$ contribution, no further higher partial waves are needed for the interpretation of these data.

3. Angular distributions

After having presented the dependence of the η production cross section on the p and q momenta, we consider here

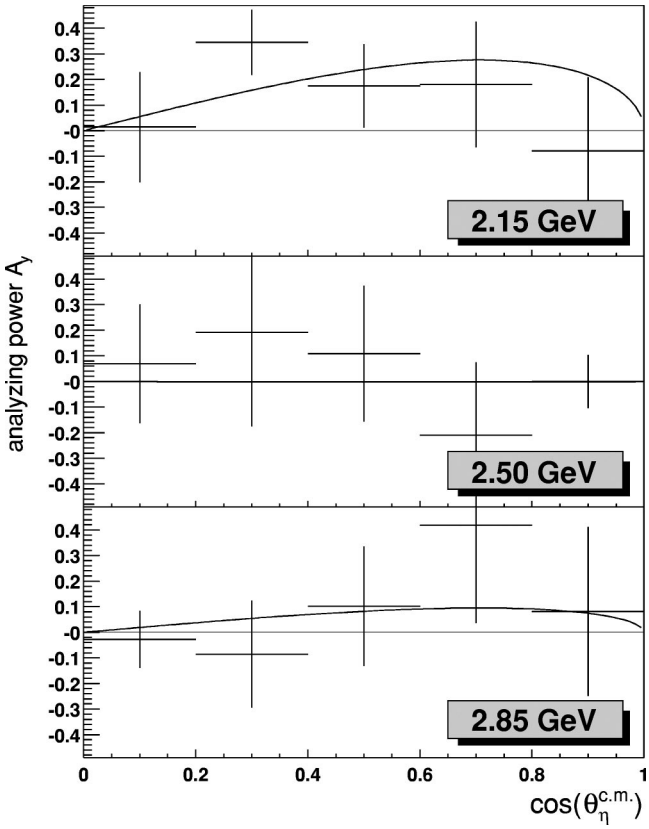

FIG. 6. Analyzing power A_y for all three beam energies as a function of $\cos(\theta_\eta^{\mathrm{c.m.}})$. The solid curves are fits to the data using formula (5).

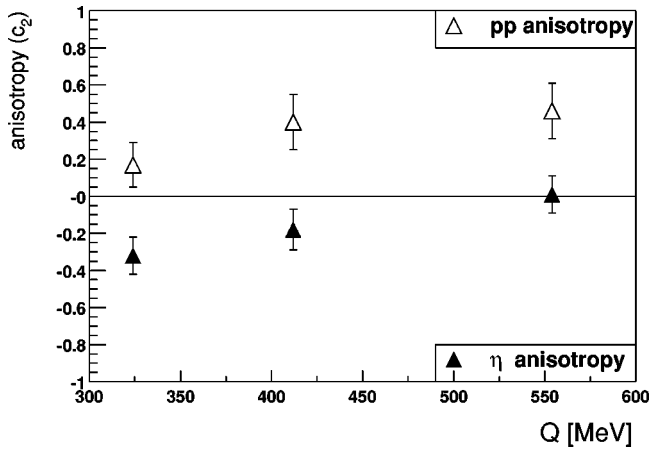

FIG. 7. The anisotropy of the η (solid data points) and the *pp* system (open data points).

TABLE III. Differential cross sections in Fig. 3.

$M^{\mathrm{inv}}_{p<\eta}$(GeV/$c^2$)	$\lvert M\rvert^2$(a.u.)
T_{beam}=2.15 GeV	
1.50	2.41±0.55
1.53	1.81±0.40
1.57	1.25±0.30
1.60	0.75±0.20
1.63	0.57±0.16
1.66	0.79±0.24
1.70	0.68±0.22
1.73	0.63±0.22
1.76	0.50±0.18
1.79	0.63±0.24
T_{beam}=2.50 GeV	
1.51	2.43±0.56
1.55	1.70±0.37
1.60	0.72±0.17
1.64	0.59±0.15
1.68	0.51±0.14
1.73	0.53±0.16
1.77	0.43±0.14
1.82	0.44±0.15
1.86	0.33±0.12
1.91	0.58±0.22
T_{beam}=2.85 GeV	
1.51	2.34±0.54
1.57	1.33±0.29
1.62	0.63±0.15
1.68	0.53±0.14
1.74	0.46±0.13
1.79	0.57±0.17
1.85	0.45±0.14
1.90	0.42±0.14
1.96	0.43±0.16

TABLE IV. Measured differential cross sections in units of μb/GeV/c.

	$T_{\rm beam}$=2.15 GeV		$T_{\rm beam}$=2.50 GeV		$T_{\rm beam}$=2.85 GeV	
q,p(GeV/c)	$d\sigma/dq$	$d\sigma/dp$	$d\sigma/dq$	$d\sigma/dp$	$d\sigma/dq$	$d\sigma/dp$
0.04	6±1	2±0	10±1	3±0	6±1	3±0
0.11	49±6	6±1	53±7	12±1	85±11	12±1
0.18	157±25	21±3	228±36	27±4	205±33	36±5
0.25	242±46	57±9	277±53	57±9	260±49	61±10
0.33	224±49	138±25	233±51	99±18	300±66	142±26
0.4	223±56	265±53	265±66	208±42	285±71	219±44
0.47	187±52	360±79	194±54	346±76	204±57	365±80
0.54	64±20	317±76	124±39	539±129	129±40	468±112
0.62	11±4	7±2	24±8	125±33	41±14	218±57
0.69	11±4	0±0	9±3	0±0	11±4	1±0

the cross section behavior as a function of the three other variables describing the $pp\eta$ final state. When integrating over both polarization states, the system has rotation symmetry around the beam axis. In that case only two angles carry significant information: $\cos\theta_\eta^{\rm c.m.}$, which is the polar angle between the η meson and the beam direction in the c.m. system (as used in our acceptance matrix), and $\cos\theta_p^{pp}$, which is the angle between the relative pp motion and the beam axis in the pp rest frame following the notation in Ref. [6]. Because the two protons are identical, we have chosen the angle of the proton in the forward hemisphere. These two angular distributions are given in Fig. 5 for each measured energy. Because $\cos\theta_p^{pp}$ is only defined between 0 and $\pi/2$, we have scaled the related differential cross sections by a factor of 1/2. Both distributions have been fit with

$$\frac{d\sigma}{d\Omega} = c_0[1 + c_2 L_2(\cos\theta)] \tag{3}$$

to evaluate the anisotropy of the angular distribution described by c_2. c_0 is a normalization factor and L_2 the second Legendre polynomial. The c_2 values for the different beam energies are listed in Table I. At the lowest beam energy, these results indicate an anisotropy of the produced η meson perpendicular to the beam direction. The anisotropy is smaller for the 2.50 GeV data and vanishes for the highest energy. The c_2 contribution of the protons has the tendency to increase with the beam energy.

4. Analyzing power

The analyzing power A_y has been evaluated by determining the η cross section after a full acceptance correction for η mesons emitted right and left of the beam, and for each beam polarization direction. Since the relative luminosity of both beam polarization directions was equal, the measured spin-dependent cross section of η mesons $\sigma_{L,R}^{\uparrow,\downarrow}$ can be directly used to calculate the analyzing power,

$$A_y = \frac{r-1}{p_b(r+1)}, \quad r = \sqrt{\frac{\sigma_L^\uparrow \sigma_R^\downarrow}{\sigma_R^\uparrow \sigma_L^\downarrow}}. \tag{4}$$

The magnitude of the vertical beam polarization is $p_b = 0.73 \pm 0.05$ for the 2.85 GeV and the 2.50 GeV beam energy, and $p_b = 0.80 \pm 0.01$ for the 2.15 GeV beam energy, determined by the proton elastic scattering. All measured A_y, summarized in Table II are consistent with zero within about 1σ. In addition, we have investigated the analyzing power as

TABLE V. Measured differential cross sections $4\pi(d\sigma/d\Omega)$ in unit of μb/sr.

	$T_{\rm beam}$=2.15 GeV		$T_{\rm beam}$=2.50 GeV		$T_{\rm beam}$=2.85 GeV	
$\cos\theta_X$	$X=\eta$	$X=pp$	$X=\eta$	$X=pp$	$X=\eta$	$X=pp$
0.05	97±10	73±7	142±14	86±9	141±14	104±10
0.15	96±10	75±7	135±15	91±9	122±13	99±10
0.25	95±11	81±8	112±13	112±11	138±16	106±11
0.35	95±12	84±8	112±14	99±20	141±18	111±11
0.45	90±12	82±8	115±15	96±10	136±18	120±12
0.55	85±12	97±10	105±15	102±10	137±19	126±13
0.65	88±13	87±9	117±17	129±13	129±19	126±13
0.75	77±12	89±18	108±17	160±32	133±21	180±36
0.85	69±11	99±30	101±16	156±31	140±23	215±43
0.95	58±10	83±17	104±17	118±35	133±22	164±49

TABLE VI. Measured analyzing power A_y.

$\cos\theta_\eta^{\text{c.m.}}$	$T_{\text{beam}}=2.15$ GeV	2.50 GeV	2.85 GeV
0.1	0.01 ± 0.22	0.07 ± 0.23	-0.02 ± 0.11
0.3	0.34 ± 0.13	0.19 ± 0.37	-0.08 ± 0.21
0.5	0.18 ± 0.16	0.11 ± 0.26	0.10 ± 0.23
0.7	0.18 ± 0.25	-0.20 ± 0.29	0.42 ± 0.38
0.9	-0.07 ± 0.29	0.00 ± 0.10	0.08 ± 0.33

a function of $\theta_\eta^{\text{c.m.}}$. Figure 6 shows the measured analyzing power A_y as a function of $\cos(\theta_\eta^{\text{c.m.}})$. The error bars reflect the individual error from the differential cross section bins and the difference between the right and left analyzing powers. The data points have been fit with

$$A_y = 2A_y^{\max}\sin\theta_\eta^{\text{c.m.}}\cos\theta_\eta^{\text{c.m.}}, \tag{5}$$

which is the predicted formula for ρ exchange [16]. All data sets are in agreement to this formula within one sigma. The results for $A_y^{\max}$ are listed in Table II. These values are compatible with zero at the two highest beam energies, whereas the analyzing power of the 2.15 GeV data shows a very slightly positive $A_y^{\max}$.

It should be noted that the analyzing power at $Q=40$ MeV seems to favor the ρ exchange [9]. Theoretical predictions on the behavior of both the $A_y(\cos\theta_\eta^{\text{c.m.}})$ and the $A_y^{\max}$ allowing a direct interpretation of our data are not yet available for higher excess energies.

III. SUMMARY AND DISCUSSION

In this paper we present the results of exclusive measurements for the reaction $\vec{p}p\to pp\eta$ at the beam kinetic energies of $T_{\text{beam}}=2.15$ GeV, 2.50 GeV, and 2.85 GeV. The relevant variables describing a three body final state were fully determined in the whole kinematic range of interest. Taking the invariant masses $M_{p_1\eta}^{\text{inv}}$ and $M_{p_2\eta}^{\text{inv}}$ we constructed the $pp\eta$ Dalitz plots that clearly show the signal from the $N(1535)S_{11}$ resonance, whose peak position and width are compatible to existing data [18,24,25]. When the η momentum in the c.m. system and the p momenta in the pp rest frame are chosen evidence for the $N(1535)S_{11}$ also appears. Beside the influence of the $N(1535)S_{11}$ and a small nonresonant contribution, no significant contributions of higher partial waves or proton-proton final state interactions can been extracted from the data.

In addition, angular distributions of differential cross sections have been investigated indicating that the polar angle anisotropy of the η in the c.m. system gradually vanishes with increasing beam energy. Moreover, the protons in the pp rest frame have the tendency to be more strongly aligned with the beam axis at higher energies, as shown in Fig. 7. The sign of the η anisotropy in our data point at $Q=324$ MeV is the same as observed in photoproduction at the MAMI [24] and GRAAL facilities [25], which corresponds to η mesons being emitted preferentially perpendicular to the beam axis. The η production anisotropy with pion beams [27], however, has the opposite sign. According to the vector dominance model, where the photon is coupling via an intermediate vector meson to the proton, this could be a hint for a dominant exchange of vector mesons for the η production in pp collisions. For a more detailed interpretation, however, theoretical effort is needed since the interference between the dominant resonant production and the small nonresonant contribution involving mesonic current may lead to a flip of the anisotropy sign [17].

For the near-threshold CELSIUS data, Fäldt and Wilkin concluded from the shape of the η angular distribution that the resonance excitation via ρ exchange is the dominant term. However, in the model of Nakayama *et al.* [17], which has been modified recently [28] to describe the new invariant mass spectra from COSY at $Q=15$ and $Q=40$ MeV [10], the dominant contribution is the exchange of pseudoscalar mesons. It should be noted that even the angular distributions from the higher statistics COSY data [10] are not sufficiently sensitive to distinguish between the model of Fäldt and Wilkin and the model of Nakayama *et al.* In this context, spin observables may help to disentangle those models, as pointed out in Refs. [17,28]. Our measured analyzing powers at all beam energies are compatible with $A_y=0$. Using the fit to the ρ exchange formula, a slight deviation from zero can be seen for the lowest beam energy.

Since the existing calculations are only done for the near-threshold regime, a direct comparison of our data with these models is not yet possible. However, the behavior of the angular distributions and the $A_y^{\max}$ of our data should be taken into account together with the new near-threshold data from COSY in upcoming model calculations. In addition, experimental effort is needed for the region of 40 MeV $<Q<300$ MeV.

ACKNOWLEDGMENTS

We acknowledge the SATURNE II accelerator staff and technical support groups for delivering an excellent proton beam and assisting this experimental program. This work was supported by CNRS-IN2P3, CEA-DSM, NSF, INFN, KBN (5P03B14020) and GSI.

APPENDIX: DATA TABLES

In this appendix the differential cross sections presented in the figures above are listed in Tables III–VI. In Tables IV and V, additional global systematic uncertainties of the absolute scale of 22%, 30%, and 33% for the $T_{\text{beam}}=2.15$ GeV, 2.50 GeV, and 2.85 GeV beam energies, respectively, have to be included.

[1] E. Pickup *et al.*, Phys. Rev. Lett. **8**, 329 (1962); G. Alexander *et al.*, Phys. Rev. **154**, 1284 (1967); A. P. Colleraine and U. Nauenberg, *ibid.* **161**, 1387 (1967); L. Bodini *et al.*, Nuovo Cimento A **58**, 475 (1968); C. Caso *et al.*, *ibid.* **55**, 66 (1968); S. P. Almeida *et al.*, Phys. Rev. **174**, 1638 (1968); E. Colton and E. Gellert, Phys. Rev. D **1**, 1979 (1970); G. Yekutieli *et al.*, Nucl. Phys. **B18**, 301 (1970).
[2] E. Chiavassa *et al.*, Phys. Lett. B **322**, 270 (1994); E. Chiavassa *et al.*, *ibid.* **337**, 192 (1994).
[3] A. M. Bergdolt *et al.*, Phys. Rev. D **48**, R2969 (1993); F. Hibou *et al.*, Phys. Lett. B **438**, 41 (1998).
[4] B. Tatischeff *et al.*, Phys. Rev. C **62**, 054001 (2000).
[5] H. Calén *et al.*, Phys. Lett. B **366**, 39 (1996); H. Calén *et al.*, Phys. Rev. C **58**, 2667 (1998).
[6] H. Calén *et al.*, Phys. Lett. B **458**, 190 (1999).
[7] A. Khoukaz *et al.*, Nucl. Phys. **A663&664**, 565c (2000); J. Smyrski *et al.*, Phys. Lett. B **474**, 182 (2000).
[8] E. Roderburg *et al.*, Acta Phys. Pol. B **31**, 2299 (2000).
[9] P. Winter *et al.*, Phys. Lett. B **544**, 251 (2002).
[10] M. Abdel-Bary *et al.*, Eur. Phys. J. A **16**, 127 (2003).
[11] J.-F. Germond and C. Wilkin, Nucl. Phys. **A518**, 308 (1990).
[12] T. Vetter, A. Engel, T. Biró, and U. Mosel, Phys. Lett. B **263**, 153 (1991).
[13] J. M. Laget, F. Wellers, and J. F. Lecolley, Phys. Lett. B **257**, 254 (1991).
[14] M. Batinić, A. Svarc, and T.S.H. Lee, Phys. Scr. **56**, 321 (1997).
[15] A. Sibirtsev and W. Cassing, nucl-th/9904046
[16] G. Fäldt and C. Wilkin, Phys. Scr. **64**, 427 (2001).
[17] K. Nakayama, J. Speth, and T.-S. H. Lee, Phys. Rev. C **65**, 045210 (2002).
[18] Particle Data Group, K. Hagiwara *et al.*, Phys. Rev. D **66**, 010001 (2002).
[19] N. Kaiser, P. B. Siegel, and W. Weise, Phys. Lett. B **362**, 23 (1995).
[20] F. Balestra *et al.*, Nucl. Instrum. Methods Phys. Res. A **426**, 385 (1999).
[21] F. Balestra *et al.*, Phys. Rev. Lett. **81**, 4572 (1998); F. Balestra *et al.*, *ibid.* **83**, 1534 (1999); F. Balestra *et al.*, Phys. Lett. B **468**, 7 (1999); F. Balestra *et al.*, Phys. Rev. Lett. **89**, 092001 (2002).
[22] F. Balestra *et al.*, Phys. Lett. B **491**, 29 (2000).
[23] F. Balestra *et al.*, Phys. Rev. C **63**, 024004 (2001).
[24] B. Krusche *et al.*, Phys. Rev. Lett. **74**, 3736 (1995); B. Krusche *et al.*, Phys. Lett. B **397**, 171 (1997).
[25] F. Renard *et al.*, Phys. Lett. B **528**, 215 (2002).
[26] R. G. Newton, *Scattering Theory of Waves and Particles* (Springer-Verlag, New York, 1982).
[27] W. Deinet *et al.*, Nucl. Phys. **B11**, 495 (1969).
[28] K. Nakayama, J. Haidenbauer, C. Hanhart, and J. Speth, Phys. Rev. C **68**, 045201 (2003).